COBEM 2021 26th International Congress of Mechanical Engineering
November 22-26, 2021, Virtual Congress, Brazil

COB-2021-0294
Passive Control of Vortex-Induced Vibrations with a Rotational Nonlinear Energy Sink

Gabriel Placeres Araujo
gabriel.pa@usp.br
José Augusto Ignácio da Silva
j.i.silva@usp.br
Flávio Donizeti Marques
fmarques@sc.usp.br

Department of Mechanical Engineering
São Carlos School of Engineering
University of São Paulo
Av. Trabalhador São-carlense, 400, 13566-590, São Carlos, SP, Brazil

Abstract. *Fluid-structure interaction vibrations are a relevant topic in several engineering fields since they can lead to structural fatigue and catastrophic failures, and their control is of significant concern. This work investigates the effects of a rotational Nonlinear Energy Sink (rotational NES) on the Vortex-Induced Vibration passive control (VIV). The NES concept has been chosen since, when properly calibrated, they can robustly suppress vibration in a wide range of excitation frequencies. The model consists of an elastically mounted cylinder subjected to transverse fluid flow. The rotational NES is attached to the cylinder as a rigid arm horizontal pendulum that can freely oscillate, thereby absorbing the cylinder vibration and passively dissipating it. The VIV fluid modeling is based on a shedding wake model consisting of an adapted Van der Pol oscillator differential equation. The study is carried through simultaneous computational simulations of the system equations of motion, and optimization is done with the Particle Swarm Method. As a result, the types of response were identified and discussed, and the system's parameter influence in the structural behavior was identified. Besides that, optimal responses to the system were found based on three different cost functions.*

Keywords: *Vortex-Induced Vibrations, Nonlinear Energy Sink, rotational NES, Nonlinear Dynamics, Passive Control*

1. INTRODUCTION

The Vortex-Induced Vibration is a self-excited and self-limited phenomenon and is known to have a complex dynamical behavior. There are different ways of studying this fluid-induced oscillation, such as Computational Fluid Dynamics (CFD) methods and experimental verification. Among them, there are the wake-oscillator models, which consists on mathematically modeling the vortex shedding through differential equations. This approach of the problem is of great interest, once it has a low computational cost and poses a good representation of the phenomenon's dynamics.

Passive suppression of oscillations by means of Nonlinear Energy Sinks have been widely studied since, when properly calibrated, they can robustly suppress oscillations in a wide range of excitation frequencies. Their mechanism of action is through the Targeted Energy Transfer (TET) phenomenon, in which the structural energy is sent to the NES and passively dissipated in a fast and irreversible way (Gendelman *et al.*, 2000; Vakakis and Gendelman, 2000). There are a great number of types of NES documented in the literature, with the most relevant being the cubic NES (Lee *et al.*, 2008), the bistable NES (Al-Shudeifat, 2014), and the rotational NES (Gendelman *et al.*, 2012).

This work investigates the passive mitigation of Vortex-Induced Vibrations by means of a rotational Nonlinear Energy Sink. The equations of motion of a cylinder under transverse wind flow with a rotational nonlinear energy sink are derived. An optimization scheme using the Particle Swarm Method is used to attain the NES parameters, viewing the reduction of the vortex-induced vibrations. Time responses and bifurcation diagrams are used to analyze the NES performance. The results confirm the benefits of the rotational NES approach in dealing with VIV phenomenon in cylinders.

2. MATHEMATICAL MODEL

The structure consists in a cylinder of diameter D and mass m. The cylinder is elastically mounted with a linear stiffness k and a viscous damping of c, constituting the primary structure, named linear oscillator (LO). The external fluid has a specific mass ρ and an uniform flow with a free stream velocity of U. The rotational NES is attached to the cylinder

as a rigid arm horizontal pendulum with an arm length of r_0, punctual mass m_n and an angular damping of c_θ. The linear oscillator is allowed to vibrate only in the direction perpendicular to the fluid-flow, $y(t)$, while the NES can oscillate in the angular displacement $\theta(t)$. A schematic representation of the system is depicted in the Fig. 1.

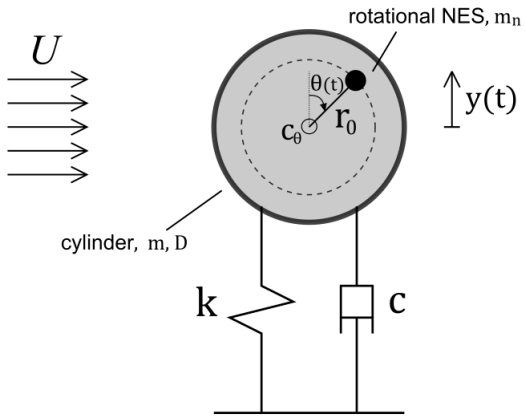

Figure 1: Schematic representation of the rotational NES attached to the linear oscillator

The equations of motion were derived through Lagrange's equations taking y and θ as generalized coordinates. The VIV effect is taken into account through the aerodynamic force $F_a(t)$, and is modeled by means of the wake model presented by Facchinetti *et al.* (2004). The wake model considers that the force $F_a(t)$ is influenced by two different contributions: the structure's drag force, proportional to the cylinder's velocity, and the vortex shedding effect, responsible for the variation of the lift coefficient. The fluctuation of the vortex street is modeled according to a modified Van der Pol oscillator dynamics by adding a third generalized coordinate, the dimensionless wake variable q, defined as $q = 2\frac{C_L(t)}{C_{L0}}$ (Dimitriadis, 2017), that relates the instantaneous lift coefficient $C_L(t)$ to the steady lift C_{L0}. Thus, the aerodynamic force is defined as: $F_a(t) = -\frac{\rho D C_D U}{2}\dot{y}(t) + \frac{\rho D C_{L0} U^2}{4} q(t)$ (Facchinetti *et al.*, 2004), where C_D is the mean sectional drag coefficient. Therefore, the set of equations of motion are:

$$\begin{cases} (m+m_n)\ddot{y}(t) + \left(c + \frac{\rho_f D C_D U}{2}\right)\dot{y}(t) + k y(t) - \frac{\rho_f D C_{L_0} U^2}{4} q(t) = m_n r_0 \frac{d}{dt}(\dot{\theta}(t)\sin(\theta(t))) \\ m_n r_0^2 \ddot{\theta}(t) + c_\theta \dot{\theta}(t) = m_n r_0 \ddot{y}(t)\sin(\theta(t)) \\ \ddot{q}(t) + \lambda\omega_f\left(q(t)^2 - 1\right)\dot{q}(t) + \omega_f^2 q(t) - \mathcal{A}_0 \frac{\ddot{y}(t)}{D} = 0 \end{cases} \tag{1}$$

where λ and $\mathcal{A}_0$ are empirical parameters and ω_f is the vortex shedding frequency defined as $\omega_f = \frac{2\pi S_t U}{D}$, with S_t being the Strouhal number.

The system defined in Eqs. (1) can be reduced by introducing the dimensionless parameters:

$$\omega = \sqrt{\frac{k}{m+m_n}}\,, \quad \zeta = \frac{c}{2(m+m_n)\omega}\,, \quad \zeta_\theta = \frac{c_\theta}{2m_n r_0^2 \omega}\,, \quad \eta = \frac{y}{D}\,,$$

$$r_r = \frac{r_0}{D}\,, \quad m_r = \frac{m_n}{m}\,, \quad \tau = \omega t\,, \quad \text{and} \quad \Omega = \frac{\omega_f}{\omega}\,,$$

which results in the following dimensionless form of Eqs. (1):

$$\begin{cases} \ddot{\eta}(\tau) + \left(2\zeta + \frac{\rho_f D C_D U}{2(m+m_n)\omega}\right)\dot{\eta}(\tau) + \eta(\tau) - \frac{\rho_f D C_{L_0} U^2}{4(m+m_n)\omega^2} q(\tau) = (\frac{m_r}{1+m_r}) r_r \frac{d}{d\tau}(\dot{\theta}(\tau)\sin(\theta(\tau))) \\ \ddot{\theta}(\tau) + 2\zeta_\theta \dot{\theta}(\tau) = \frac{1}{r_r}\ddot{\eta}(\tau)\sin(\theta(\tau)) \\ \ddot{q}(\tau) + \lambda\Omega\left(q(\tau)^2 - 1\right)\dot{q}(\tau) + \Omega^2 q(\tau) - \mathcal{A}_0\ddot{\eta}(\tau) = 0 \end{cases} \tag{2}$$

3. SIMULATION METHODOLOGY

The dimensionless equations of motion (*cf.* Eqs. (2)) were numerically simulated through the Runge-Kutta method. The total simulation dimensionless time was defined as $\tau = 2000$ with a time-step of $\Delta\tau = 0.1$. The initial conditions were taken as $\eta(0) = 0.01$, $\dot{\eta}(0) = 0$, $\theta = \pi/2$, $\dot{\theta} = 0$, $q(0) = 0$, and $\dot{q}(0) = 0$, for all cases in this work. The cylinder structure is assumed to have the same parameters as the one studied by Dai *et al.* (2017) for the cubic NES, that is: $m = 0.044$ kg/m, $\omega = 62.8$ rad/s, and $\zeta = 0.0013$. The airflow is considered with a density of 1.225 kg/m^3, and the

aerodynamic coefficients of $C_D = 1.2$ and $C_{L0} = 0.3$ (Facchinetti *et al.*, 2004). For the vortex shedding model, it is used the parameters of $S_t = 0.2$, $\lambda = 0.24$, and $\mathcal{A}_0 = 15$, which are the same values used by Dai *et al.* (2017).

The NES' mass ratio m_r deeply influences the behavior of the system, once it changes the linear oscillator's natural frequency and the VIV phenomenon is observed to be particularly sensitive to changes in its reduced mass parameter m^* (the ratio of the structural mass to the displaced fluid mass, defined as $m^* = \frac{m+m_n}{m_f} = \rho L \pi (\frac{D^2}{4})$) (Khalak and Williamson, 1999). In order to bypass that limitation, it is assumed that the primary structure has a fixed linear stiffness k with a varying natural frequency, which is dependent of the mass ratio and the cylinder's fundamental frequency ω. Thus, every simulation is done considering the total mass with the NES in its resonance frequency and is compared to the system with the absorber attached but unable to rotate.

The optimization was done through the Particle Swarm Method. The damping ratio was fixed as $\zeta = 0.1$ and the optimization algorithm was allowed to change parameters of m_r and r_r. The boundaries for the optimization parameters were set as $r_r \in [0.05, 0.5]$ and $m_r \in [0.01, 0.3]$. In order to find the optimal response of the system, three cost functions were defined based on the total mechanical energy of the system, the percentage of instantaneous energy in the NES and a criterion of suppression efficiency introduced by Ueno and Franzini (2019), which is presented by:

$$S = 1 - \frac{A_{NES}}{A_{LO}} \quad , \tag{3}$$

where A_{NES} is the amplitude of the cylinder with the NES, and A_{LO} is the amplitude of the cylinder without NES for the same condition.

The criterion in Eq. (3) is based on the characteristic oscillation amplitude for both the controlled and uncontrolled system and the closer it is 1, greater is the vibration mitigation. The characteristic amplitudes were computed as being $A = \sqrt{2} std(y_{pr})$, with y_{pr} being the vertical vibration in permanent regime, assumed as happening from the dimensionless time $\tau = 1000$.

4. RESULTS AND DISCUSSION

In this section, the results of the simulations will be presented and discussed. For better visualization, it will be divided in three subsections, where the possible types of dynamical responses will be shown, the influence of the NES parameters will be discussed and the obtained optimized system will be presented.

4.1 Types of Responses

Throughout the simulations, five types of responses were identified: the locked stable NES, the oscillatory regime, the Strongly Modulated Response (SMR), the constant-speed rotational response and the chaotic behavior.

The locked stable NES regime occurs when, after a transient, the NES stops its movement in a stable position, usually in $\theta = 0$. Thus, it stops the absorption of energy from the primary structure and presents a highly inefficient behavior, unable to mitigate the linear oscillator's vibration. An example of such a behavior is shown in Fig. 2.

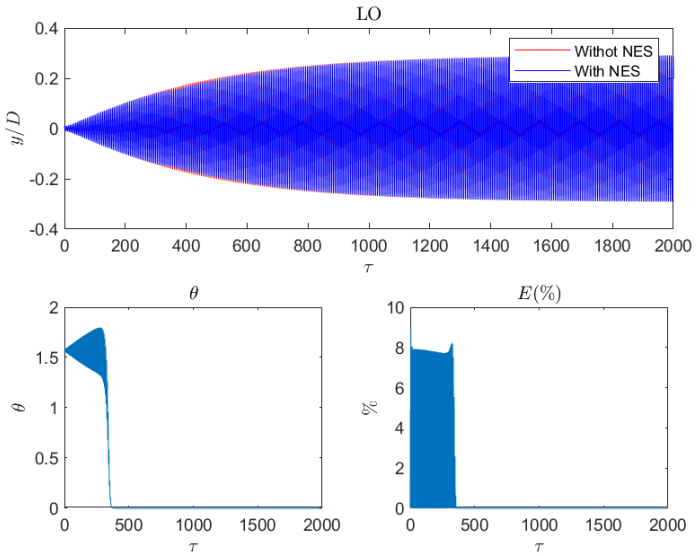

Figure 2: Example of locked stable regime for parameters of: $m_r = 0.1$, $r_r = 0.5$ and $\zeta_\theta = 0.2$.

In the oscillatory regime, the NES has a periodic oscillation around an stable position. When properly calibrated, this

behavior can passively suppress the primary structure's vibration, but usually with a low efficiency, once low percentages of energy are transferred to the absorber. This regime is depicted in the Fig. 3.

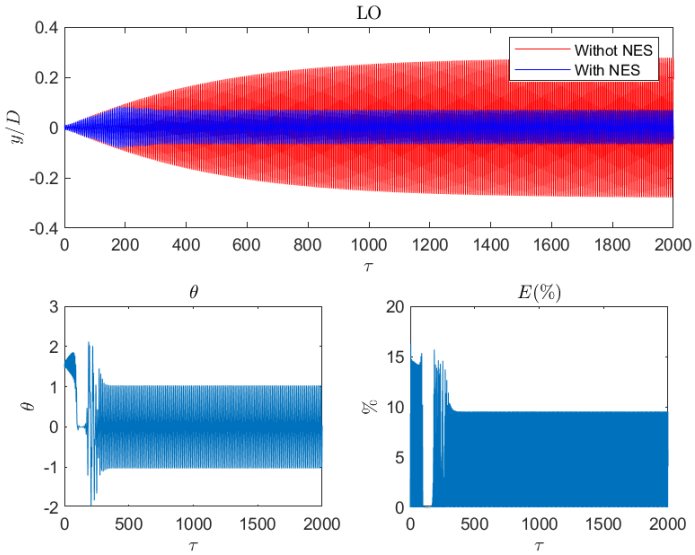

Figure 3: Example of periodic oscillatory regime for parameters of: $m_r = 0.2$, $r_r = 0.1$ and $\zeta_\theta = 0.2$.

The Strongly Modulated Response (SMR) is widely studied in the literature and is a common response between the different configurations of Nonlinear Energy Sinks. It is observed to efficiently suppress the vibration through the TET phenomenon. In the rotational NES, it occurs when the rotational movement of the NES alternates cyclically between constant-speed movement (when the energy is transferred to the NES) and zero-speed regions (when the energy sent to the absorber is totally dissipated). An example of SMR is depicted in Fig. 4.

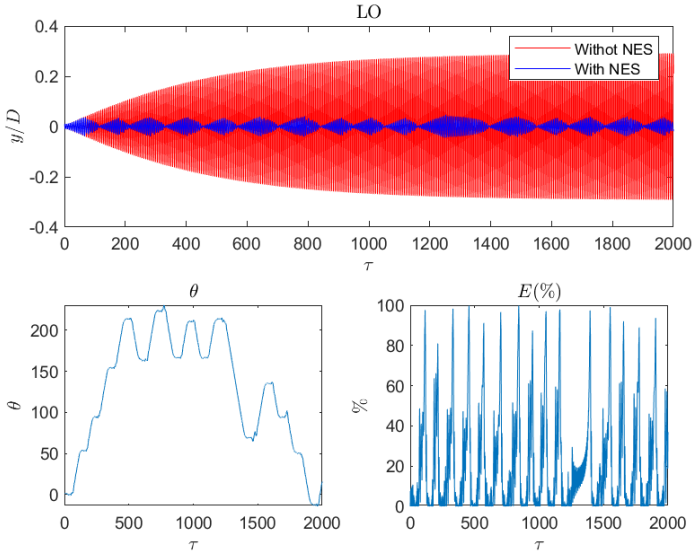

Figure 4: Example of SMR for parameters of: $m_r = 0.1$, $r_r = 0.05$ and $\zeta_\theta = 0.05$.

The constant-speed rotational behavior happens when the energy transferred to the NES implies in its full rotation with a near constant speed. This is usually followed by high percentages of the total mechanical energy sent to the NES. This regime is pictured in the Fig. 5. It is observed that when the NES engages in the full rotation regime, the Linear Oscillator's vibration reduces and is efficiently mitigated.

Lastly, the chaotic response happens when the system runs in a disorganized way. Little energy is transferred to the NES and it is noticed to have an inefficient vibration mitigation of the primary structure. This regime is presented in the Fig. 6.

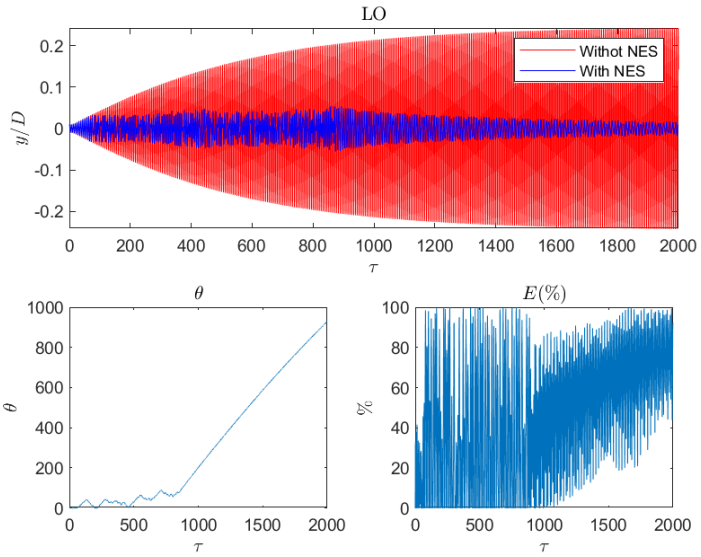

Figure 5: Example of constant-speed rotational regime for parameters of: $m_r = 0.5$, $r_r = 0.05$ and $\zeta_\theta = 0$.

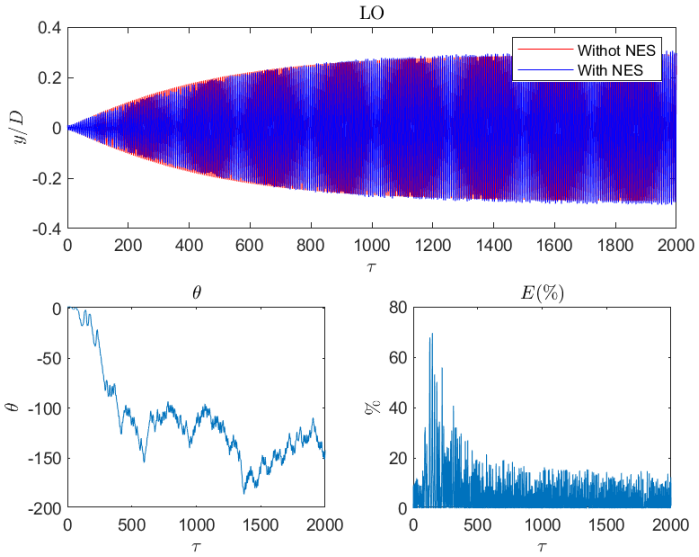

Figure 6: Example of chaotic regime for parameters of: $m_r = 0.1$, $r_r = 0.1$ and $\zeta_\theta = 0$.

4.2 Influence of the parameters of the NES

In this section, the influence of NES parameters of mass ratio m_r and radius ratio r_r are discussed. For that, bifurcations diagrams were plotted for varying values of parameters.

The study of the influence of the radius ratio r_r was done by fixing the NES mass ratio as $m_r = 0.3$ and the angular damping ratio as $\zeta_\theta = 0.1$. Thus, the bifurcation diagrams for varying radius ratios were plotted as presented in Fig. 7. It is noticed that the vibration mitigation has an inverse relation with the radius ratio, once it is greater for lower values of r_r. Despite lower values of r_r imply in greater vibration mitigation, this is a condition that is not always possible in terms of project, once the cylinders dimensions might make it impossible to be applied. Nonetheless, even greater radius ratios are observed to present good suppression behavior.

For the study of the influence of the mass ratio m_r, it was defined a radius ratio of $r_r = 0.05$ and a NES damping ratio of $\zeta_\theta = 0.1$. The bifurcation diagrams for varying mass ratios are depicted in Fig. 8. It is noticed that the behavior of the NES has a less expressive relation with its mass when compared to the NES radius. For crescent values of m_r it is observed an decrease in the vibration amplitude. However, the increase of the structure's mass is normally undesired, and, when projecting an rotational absorber, the maximum acceptable increase of mass is need to be defined. Despite that, even small mass ratio parameter's present great vibration mitigation when compared with the uncontrolled oscillation of the cylinder.

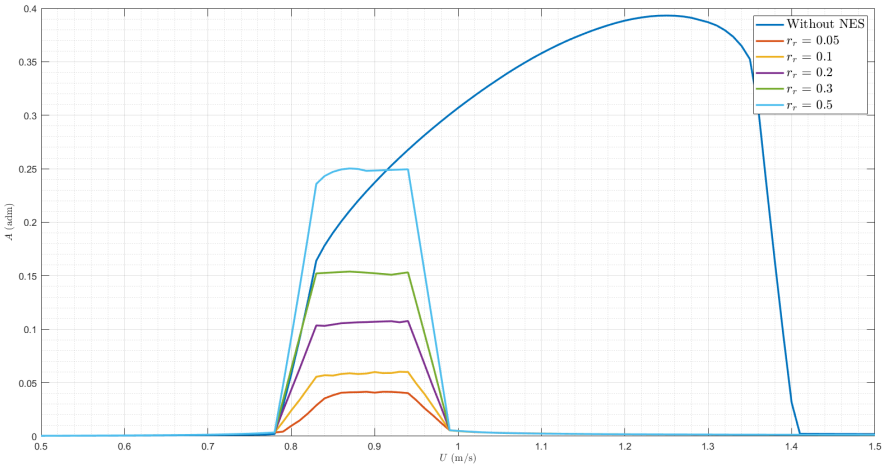

Figure 7: Bifurcation diagram for various NES' radius ratio parameters (r_r).

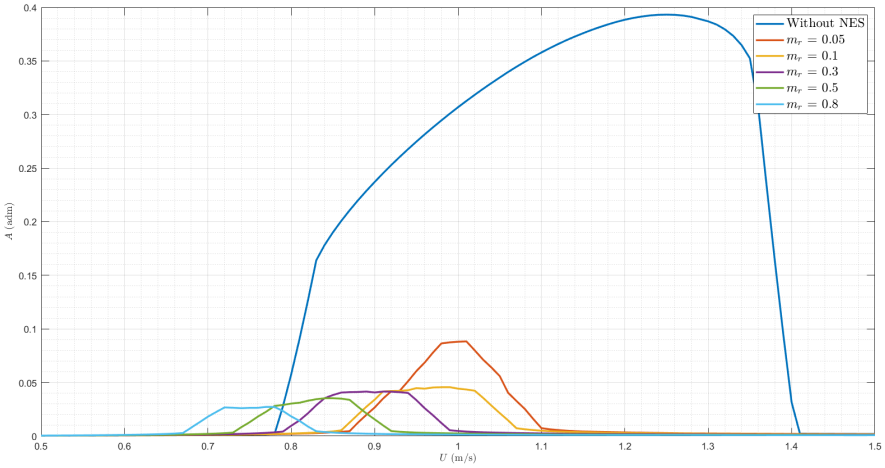

Figure 8: Bifurcation diagram for various NES' mass ratio parameters (m_r).

It is worth mentioning that the bifurcation diagrams move to the left as the mass is increased, once it changes the structural natural frequency and, thus, the fluid free stream speed that leads to structural resonance. It is also observed that the vibration amplitude has a greater relation with its radius ratio r_r than the mass ratio m_r. The optimal responses are, thus, probably found in low radius and high mass NES configurations.

4.3 Optimizing the NES' parameters

The optimization was carried through three different cost functions: to minimize the mean total instantaneous energy of the system, maximize the S efficiency criterion and maximize the mean percentage of energy sent to the NES in permanent regime. The obtained results are depicted in Fig. 9.

All three results are observed to have Strongly Modulated Responses (SMR) with a high oscillation mitigation. This result is coherent to the literature observation, once the TET phenomenon is noticed to happen greatly in this kind o response. Furthermore, the responses obtained in Figs. 9b and 9c have really similar parameter, with the mass ratio near the upper limit of the optimization and percentage of energy sent to the NES close to the 100% in some modulations. As previously discussed, all simulations found its optimal responses in the minimum radius ratio allowed, $r_r = 0.05$.

Figure 10 depicts the bifurcation diagram of the three optimal systems obtained compared to the uncontrolled Linear Oscillator vibration. It is noticed that the curve that presents the best behavior is the efficiency factor S, once it has a similar suppression of oscillation with a lower mass. It is worth commenting that the optimal systems based on the percentage of energy and the total energy sent to the NES have a mass ratio near the upper boundary set of $m_r = 0.3$. Although in a simulation with a higher boundary the existence of an other optimal system is possible, it is possibly inadvisable in a real project, once it would imply in a greater mass.

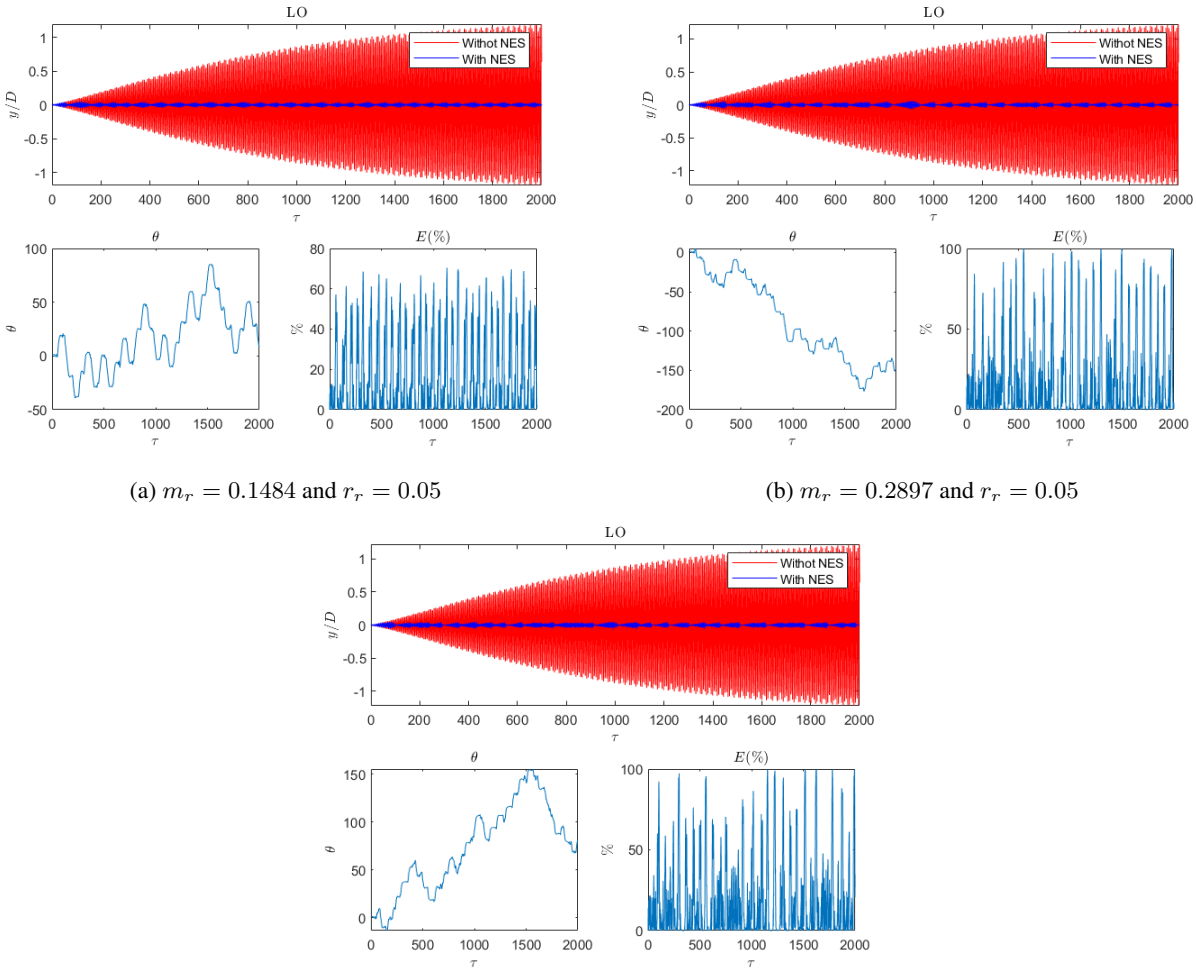

(a) $m_r = 0.1484$ and $r_r = 0.05$

(b) $m_r = 0.2897$ and $r_r = 0.05$

(c) $m_r = 0.2826$ and $r_r = 0.05$

Figure 9: Optimization results for the: (a) mean total energy, (b) S efficiency criterion, (c) percentage of energy sent to the NES.

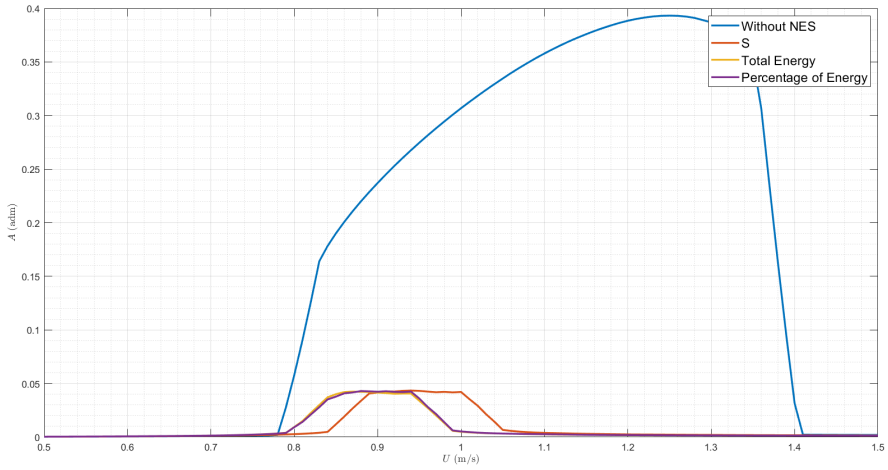

Figure 10: Bifurcation diagrams for the three optimal systems based on the total energy, the S criterion and the percentage of energy sent to the NES.

5. CONCLUSION

This work presented a study on the passive suppression of Vortex-Induced Vibrations by means of a rotational Nonlinear Energy Sink. The system simulated consists of an elastically mounted cylinder engaging a 1-dof oscillation. The NES

was attached as a rigid arm horizontal pendulum allowed to rotate freely and dissipate energy through angular damping. The fluid-structure interaction was modeled by means of a wake oscillator model due to its low computational cost and a good representation of the VIV phenomenon. The simulations were done through direct time integration of the nonlinear differential equations, and optimization was done through the Particle Swarm Method.

As a result, five types of response were identified in the system, with emphasis on the Strongly Modulated Response, which turned out to be the most effective. The other types of responses obtained were: the locked stable, periodic oscillatory, constant-speed rotational, and chaotic regimes. The influence of NES parameters was studied with the analysis of bifurcation diagrams of the phenomenon for varying mass ratios m_r and radius ratios r_r. The radius was observed to be most relevant to the system dynamics, raising the oscillation mitigation for lower values of r_r.

Lastly, optimal responses were obtained by varying parameters of m_r and r_r with three different cost functions, chosen to minimize the mean total energy, maximize the S criterion, and maximize the mean percentage of energy sent to the NES. All three results obtained depicted SMR regimes with great mitigation of the structural oscillation. The optimal systems were compared and analyzed in a bifurcation diagram.

6. ACKNOWLEDGMENTS

The authors acknowledge the financial support for this investigation from the Brazilian's National Council for Scientific and Technological Development (CNPq grant #306824/2019-1), and the São Paulo State Research Foundation (FAPESP grants #2020/15610-2 and #2019/05410–9).

7. REFERENCES

Al-Shudeifat, M., 2014. "Highly efficient nonlinear energy sink". *Nonlinear Dynamics*, Vol. 76, No. 4, p. 1905 – 1920.

Dai, H.L., Abdelkefi, A. and Wang, L., 2017. "Vortex-induced vibrations mitigation through a nonlinear energy sink". *Communications in Nonlinear Science and Numerical Simulation*, Vol. 42, pp. 22–36. doi: 10.1016/j.cnsns.2016.05.014.

Dimitriadis, G., 2017. *Introduction to Nonlinear Aeroelasticity*. Aerospace Series. Wiley. ISBN 9781118613474.

Facchinetti, M., de Langre, E. and Biolley, F., 2004. "Coupling of structure and wake oscillators in vortex-induced vibrations". *Journal of Fluids and Structures*, Vol. 19, No. 2, pp. 123–140. ISSN 0889-9746. doi: 10.1016/j.jfluidstructs.2003.12.004.

Gendelman, O., Manevitch, L.I., Vakakis, A.F. and M'Closkey, R., 2000. "Energy pumping in nonlinear mechanical oscillators: Part i — dynamics of the underlying hamiltonian systems". *Journal of Applied Mechanics*, Vol. 68, No. 1, pp. 34 – 41.

Gendelman, O., Sigalov, G., Manevitch, L., Mane, M., Vakakis, A. and Bergman, L., 2012. "Dynamics of an eccentric rotational nonlinear energy sink". *Journal of Applied Mechanics*, Vol. 79, No. 1, p. 011012.

Khalak, A. and Williamson, C.H.K., 1999. "Motions, forces and mode transitions in vortex-induced vibrations at low mass-damping". *Journal of Fluids and Structures*, Vol. 13, No. 7, pp. 813–851. doi:10.1006/jfls.1999.0236.

Lee, Y., Vakakis, A., Bergman, L., Mcfarland, D., Kerschen, G., Nucera, F., Tsakirtzis, S. and Panagopoulos, P., 2008. "Passive non-linear targeted energy transfer and its applications to vibration absorption: A review". *Proceedings of The Institution of Mechanical Engineers Part K-journal of Multi-body Dynamics*, Vol. 222, No. 2, pp. 77 – 134.

Ueno, T. and Franzini, G.R., 2019. "Numerical studies on passive suppression of one and two degrees-of-freedom vortex-induced vibrations using a rotative non-linear vibration absorber". *International Journal of Non Linear Mechanics*, Vol. 116, pp. 230–249. doi:10.1016/j.ijnonlinmec.2019.07.001.

Vakakis, A.F. and Gendelman, O., 2000. "Energy pumping in nonlinear mechanical oscillators: Part ii — resonance capture". *Journal of Applied Mechanics*, Vol. 68, No. 1, pp. 42 – 48.

8. RESPONSIBILITY NOTICE

The authors are solely responsible for the printed material included in this paper.